THE JOURNAL OF PHYSICAL CHEMISTRY C

Article

pubs.acs.org/JPCC

Spectroscopic Characterization and Modeling of Methyl- and Hydrogen-Terminated Oligo(ethylene glycol) Self-Assembled Monolayers

Lyuba Malysheva,[†,‡] Alexander Onipko,[‡] Timmy Fyrner,[§] Hung-Hsun Lee,[∥] Ramūnas Valiokas,[⊥] Peter Konradsson,[§] and Bo Liedberg*[,∥]

[†]Bogolyubov Institute for Theoretical Physics, 03680 Kiev, Ukraine

[‡]Laboratory on Quantum Theory in Linköping, Box 8017, SE-580 08 Linköping, Sweden

[§]Division of Organic Chemistry, Department of Physics, Chemistry, and Biology, Linköping University, SE-581 83 Linköping, Sweden

[∥]Division of Molecular Physics, Department of Physics, Chemistry, and Biology, Linköping University, SE-581 83 Linköping, Sweden

[⊥]Department of Nanoengineering, Center for Physical Sciences and Engineering, Savanoriu 231, LT-02300 Vilnius, Lithuania

ABSTRACT: Two series of oligo(ethylene glycol) (OEG) thiol compounds HS-$(CH_2CH_2O)_nR$, with R = CH_3, H and n = 5, 6, 7, have been synthesized and used to form self-assembled monolayers (SAMs) on gold. The data from null ellipsometry, infrared reflection−absorption spectroscopy, and ab initio calculations of this type of OH- and CH_3-terminated OEG SAMs are used to examine the rarely addressed in-SAM orientation of oligo(ethylene glycols) and to provide detailed assignments of infrared bands in the fingerprint and CH-stretching regions. On the basis of these results, a new spectral band has been observed at 2947 cm^{-1} and identified by the first-principle calculations as localized vibrations that are specific for hydrogen-terminated OEG thiolate SAMs. This band can be used as an indicator of a high crystalline-like ordering. It is furthermore stressed that theory agrees with the experimentally obtained CH-stretching spectra remarkably well if, and only if, the OEG helix axis within studied SAMs is tilted by about 20° with respect to the surface normal.

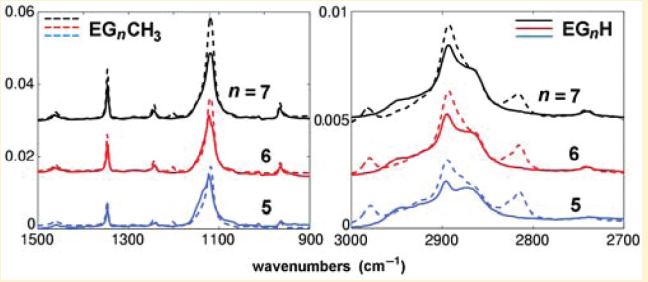

INTRODUCTION

Self-assembled monolayers (SAMs) bearing short oligo(ethylene glycols) (OEGs)[1−3] have become a common surface platform in biomedical and bioanalytical research and applications. In this context, the conformational flexibility and unique resistance of OEGs to nonspecific binding of proteins and cells is combined with the high structural order, Å-precision in positioning of chemical groups across the interface, and the relatively high stability of SAMs on metal and oxide surfaces.

Over the past decades, OEG-terminated and OEG-containing alkylthiolate SAMs on gold have been extensively studied experimentally and theoretically by many groups (see refs 1−17). These studies revealed more complex structural characteristics and phase behavior of OEG SAMs as compared to the regular ω-substituted alkanethiolate SAMs. For example, EG_n moieties with $n \geq 3$ can be switched between helical and all-trans conformations by metallic lattice,[4] synthetic design,[11] and/or temperature.[18,19] In addition, the specific interactions of helical, all-trans, and amorphous OEG conformations with water molecules have been suggested as the key factor determining the performance of OEG-terminated assemblies in terms of the nonspecific protein binding and antifouling.[6,20,21]

To investigate the above-mentioned and other structural aspects of OEG SAMs, a variety of self-assembling compounds have been prepared. Besides, the structural properties, the synthetic designs, and preparation protocols are important for the fabrication of biospecific surfaces and soft micro/nanostructures. Namely, compounds with different molecular weight (variation in the length of the alkyl spacer, the OEG portion and/or presence of functional chemical groups, etc.) can be assembled by using specific deposition protocols and patterning tools. For instance, Tampé et al. recently showed that 11-(mercaptoundecyl)-triethylene glycol SAMs can be grown from vapor phase.[22] Similar tri(ethylene glycol) thiol derivatives with a short alkyl spacer have been used as a bioinert molecular resist for scanning probe nanolithography on gold.[23] Moreover, the length of the SAM-forming OEG molecules was found to be an important factor for minimizing viscoelastic interference at biosensor surfaces for quartz crystal micro-

Received: December 22, 2011
Revised: May 8, 2012
Published: May 15, 2012

   dx.doi.org/10.1021/jp212400z | J. Phys. Chem. C 2012, 116, 12008−12016

balance with dissipation monitoring (QCM-D).[24] For this reason, in QCM-D biosensing applications, short OEG compounds without the alkyl spacer are preferred.[25]

In our previous studies, we have shown that variations in the length of the OEG and alkyl portions and proper choice of linkage groups, respectively, results in significant differences in the conformation of the constituent molecules and the overall order and phase behavior of the SAMs.[17] In these and in the overwhelming majority of other works, characterization has been performed by means of infrared (IR) reflection–absorption (RA) spectroscopy, the most commonly used technique for conformational analysis of thin film and monolayer architectures. However, basic information, such as the OEG chain tilt angle θ, still remains an open question, despite its importance for gaining a deeper understanding of the spectral appearance of CH-stretching vibrations and signatures of other IR-active characteristic vibrations. In an attempt to fill the gap, we have already examined a wealth of experimental data combined with ab initio modeling and argued that, for both OEG-terminated alkylthiolate SAMs[13] and alkyl-terminated OEG SAMs on gold,[16] $\theta \approx 20°$. To further elaborate on this issue, we examine in this report the spectroscopic consequences of either an up-right or tilted OEG axis with respect to the SAM-supporting gold surface. We come to the conclusion that an upright orientation is not consistent neither with the observed nor model spectra, particularly, in the CH-stretching region of the IR-RA spectra. In what follows, we discuss two SAM series of alkyl-free OEG thiols, HS-$(CH_2CH_2O)_n$R with R = CH_3, H and n = 5, 6, 7 (both termini have been previously used in protein resistance studies[4,26]). Basic infrared and ellipsometric characterization has resulted in a substantially improved understanding of the spectral appearance of pure OEG SAMs and the dependence on the OEG length, terminal group, and chain orientation. We discuss the results obtained by means of infrared spectroscopy and ab initio calculations, providing an interpretation of CH-stretching spectra that, in part, can be regarded as nontraditional.

EXPERIMENTAL SECTION

Synthesis. *General Methods.* Normal workup means drying the organic phase with $MgSO_4$(s), filtering, and concentration in vacuum below 40 °C. TLC was performed on silica gel F_{254} plates and detected by I_2(s) or by charring with PAA [EtOH (95%), H_2SO_4, *p*-anisaldehyde, and acetic acid, 90:3:2:1] followed by heating at ∼250 °C. Silica gel (0.040–0.063 mm) was used for Flash Chromatography (FC). NMR spectra were recorded on a Varian Mercury 300 (^{1}H 300 MHz and ^{13}C 75.4 MHz) instrument at 25 °C. ^{1}H and ^{13}C chemical shifts are given in ppm relative to TMS (δ 0.00) in $CDCl_3$. MALDI-TOF mass-spectra were recorded with a Voyager-DE STR Biospectrometry Workstation, in positive mode, using an α-cyano-4-hydroxycinnamic acid matrix and the dimer (m/z 379.0930) as internal standard.

General Procedures. The substitution and deprotection procedure is outlined in Scheme 1. (I) (substitution): To a mixture of **1a** (1 equiv) and DMAP (0.1 equiv) in CH_2Cl_2/pyridine was added TsCl (2 equiv). The solution was stirred overnight, diluted with CH_2Cl_2, and washed with 1 M HCl (aq.), $NaHCO_3$ (sat. aq.), and H_2O. Normal workup gave the crude tosylate, which, without further purification, was dissolved in dry DMF. KSAc (1.5 equiv) was added, and the solution was stirred for 2 h, diluted with CH_2Cl_2, and washed with brine and H_2O. Normal workup followed by FC gave the acetylated derivative **1b**. (II) (deprotection): To a mixture of **1b** (1 equiv) in MeOH was added NaOMe (5 equiv). The solution was stirred for 1.5 h, neutralized with DOWEX-H^+, filtered, and concentrated. FC gave the thiol derivative **1c**.

Scheme 1[a]

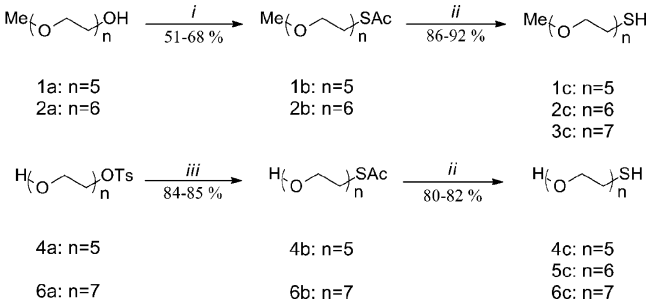

[a](i) (a) TsCl, DMAP, CH_2Cl_2/pyridine (1:2), (b) KSAc, DMF; (ii) NaOMe, MeOH; (iii) KSAc, DMF.

14-Acetylthio-1-methoxy-3,6,9,12-tetraoxatetradecane-[Me(OCH$_2$CH$_2$)$_5$SAc] ***1b***. Compound **1b** was synthesized according to general procedure (I) using **1a**. FC (EtOAc) gave **1b** (0.13 g, 0.41 mmol, 68%) as colorless oil. R_f = 0.67 (EtOAc/MeOH 9:1). NMR: ^{1}H (300 MHz, $CDCl_3$), δ 2.30 (s, 3 H, C$\underline{H}_3$), 3.06 (t, 2 H, J = 6.4 Hz, C$\underline{H}_2$SAc), 3.35 (s, 3 H, OC$\underline{H}_3$), 3.50–3.64 (m, 18 H); ^{13}C (75.4 MHz, $CDCl_3$), δ 28.9, 30.6, 59.1, 69.8, 70.4–70.7 (several peaks), 72.0, 195.5. MALDI-TOF calcd for $C_{13}H_{26}NaO_6S$, $[M + Na]^+$ 333.2; found, $[M + Na]^+$ 333.2.

14-Methoxy-3,6,9,12-tetraoxatetradecanethiol [Me-(OCH$_2$CH$_2$)$_5$SH] ***1c***.[9] Compound **1b** was deprotected according to general procedure (II). FC (EtOAc) gave **1c** (0.10 g, 0.38 mmol, 92%) as colorless oil. R_f = 0.63 (EtOAc/MeOH 9:1). NMR: ^{1}H (300 MHz, $CDCl_3$), δ 2.68 (dt, 2 H, J = 8.2, 6.4 Hz, C$\underline{H}_2$SH), 3.37 (s, 3 H, OC$\underline{H}_3$), 3.52–3.66 (m, 18 H); ^{13}C (75.4 MHz, $CDCl_3$), δ 24.3, 59.1, 70.3, 70.6–70.7 (several peaks), 72.0, 73.0. MALDI-TOF calcd for $C_{11}H_{24}NaO_5S$, $[M + Na]^+$ 291.1; found, $[M + Na]^+$ 291.2.

17-Acetylthio-1-methoxy-3,6,9,12,15-pentaoxaheptadecane [Me(OCH$_2$CH$_2$)$_6$SAc] ***2b***. Compound **2b** was synthesized according to general procedure (I) using **2a**. FC (EtOAc) gave **2b** (0.12 g, 0.33 mmol, 51%) as a colorless oil. R_f = 0.58 (EtOAc/MeOH 9:1). NMR: ^{1}H (300 MHz, $CDCl_3$), δ 2.30 (s, 3 H, C$\underline{H}_3$), 3.05 (t, 2 H, J = 6.5 Hz, C$\underline{H}_2$SAc), 3.33 (s, 3 H, OC$\underline{H}_3$), 3.49–3.62 (m, 22 H); ^{13}C (75.4 MHz, $CDCl_3$), δ 28.9, 30.6, 59.1, 69.8, 70.4–71.7 (several peaks), 71.4, 72.0, 195.5. MALDI-TOF calcd for $C_{15}H_{30}NaO_7S$, $[M + Na]^+$ 377.2; found, $[M + Na]^+$ 377.1.

17-Methoxy-3,6,9,12,15-pentaoxaheptadecanethiol [Me-(OCH$_2$CH$_2$)$_6$SH] ***2c***.[8] Compound **2b** was deprotected according to general procedure (II). FC (EtOAc) gave **2c** (89 mg, 0.29 mmol, 86%) as a colorless oil. R_f = 0.53 (EtOAc/MeOH 9:1). NMR: ^{1}H (300 MHz, $CDCl_3$), δ 2.68 (dt, 2 H, J = 8.2, 6.5 Hz, C$\underline{H}_2$SH), 3.36 (s, 3 H, OC$\underline{H}_3$), 3.51–3.73 (m, 22 H); ^{13}C (75.4 MHz, $CDCl_3$), δ 24.4, 59.1, 70.3, 70.6–70.7 (Several peaks), 72.0, 73.1. MALDI-TOF calcd for $C_{13}H_{28}NaO_6S$, $[M + Na]^+$ 335.2; found, $[M + Na]^+$ 335.2.

20-Methoxy-3,6,9,12,15,18-hexaoxaeicosanethiol [Me-(OCH$_2$CH$_2$)$_7$SH] ***3c***. Compound **3c** was synthesized according to Saalmink et al.[27]

14-Acetylthio-3,6,9,12-tetraoxatetradecane [H-(OCH$_2$CH$_2$)$_5$SAc] ***4b***. To a mixture of $[H(OCH_2CH_2)_5OTs]$

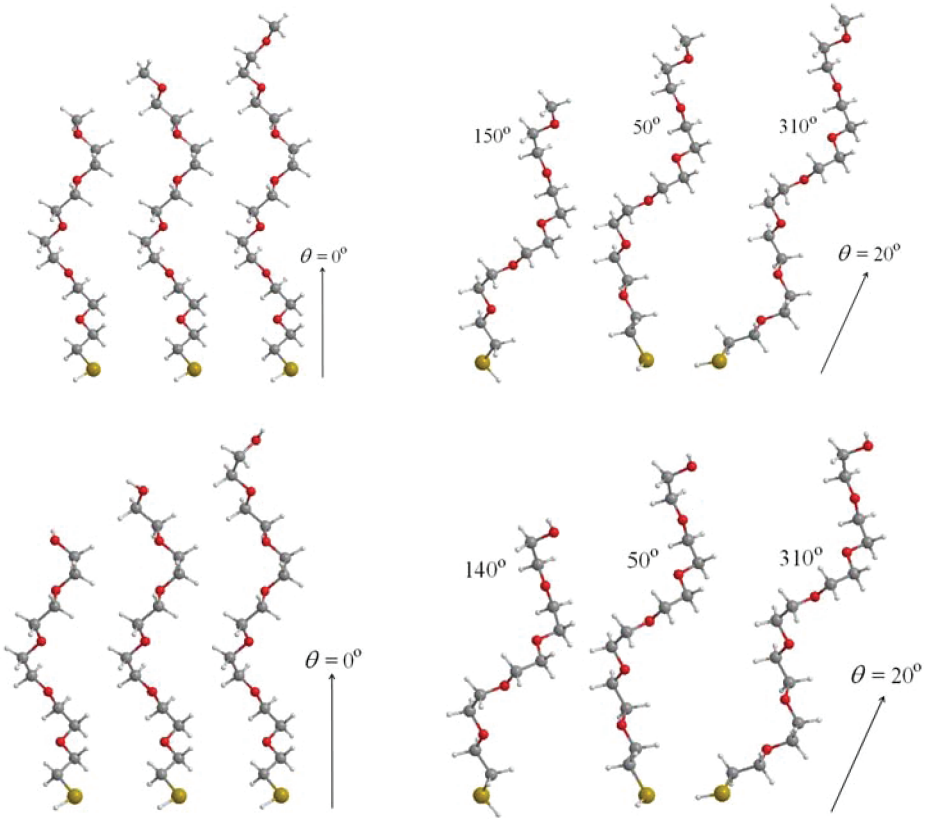

Figure 1. Optimized geometries of molecules HS-EG$_n$CH$_3$ (above) and HS-EG$_n$H (below), n = 5, 6, 7. Molecules in the upright position with zero tilt (θ) and rotation (ψ) angles are shown on the left. On the right, θ = 20°, and ψ = 140° (H terminus) and 150° (CH$_3$ terminus) for n = 5, ψ = 50° for n = 6, and ψ = 310° for n = 7. These are orientations of SAM constituents giving the model IR-RA spectra represented in Figure 2. Values of angle ψ label the correspondingly rotated molecules with different number of EG units.

4a[28,29] (0.36 g, 0.92 mmol) in dry DMF (5 mL) was added KSAc (0.16 g, 1.4 mmol). The solution was stirred for 1 h and coevaporated with toluene. FC (EtOAc) gave **4b** (0.23 g, 0.77 mmol, 84%) as colorless oil. R_f = 0.59 (EtOAc/MeOH 10:1). NMR: ^{1}H (300 MHz, $CDCl_3$), δ 2.30 (s, 3 H, C$\underline{H}_3$), 3.05 (t, 2 H, J = 6.4 Hz, C$\underline{H}_2$SAc), 3.54−3.69 (m, 18 H); ^{13}C (75.4 MHz, $CDCl_3$), δ 28.9, 30.6, 61.8, 69.8, 70.4, 70.4, 70.6−70.7 (several peaks), 72.6, 195.6. MALDI-TOF calcd for $C_{12}H_{24}NaO_6S$, [M + Na]$^+$ 319.1; found, [M + Na]$^+$ 319.2.

14-Thio-3,6,9,12-tetraoxatetradecane-1-ol[H-(OCH$_2$CH$_2$)$_5$SH] ***4c***. Compound **4b** was deprotected according to general procedure (II). FC gave **4c** (0.12 g, 0.46 mmol, 80%) as colorless oil. R_f = 0.52 (EtOAc/MeOH 10:1). NMR: ^{1}H (300 MHz, $CDCl_3$), δ 2.67 (dt, 2 H, J = 6.4, 8.2 Hz, C$\underline{H}_2$SH), 3.56−3.71 (m, 18 H); ^{13}C (75.4 MHz, $CDCl_3$), δ 24.3, 61.8, 70.3, 70.5, 70.6−70.7 (several peaks), 72.6, 73.0. MALDI-TOF calcd for $C_{10}H_{22}NaO_5S$, [M + Na]$^+$ 277.0; found, [M + Na]$^+$ 277.1.

17-Thio-3,6,9,12,15-pentaoxaheptadecanethiol [HO-(OCH$_2$CH$_2$)$_6$SH] ***5c***. Compound **5c** was synthesized according to Boden et al.[30]

20-Acetylthio-3,6,9,12,15,18-hexaoxaeicosan-1-ol [H-(OCH$_2$CH$_2$)$_7$SAc] ***6b***. To a mixture of [H(OCH$_2$CH$_2$)$_7$OTs] **6a**[31] (0.14 g, 0.29 mmol) in dry DMF (2 mL) was added KSAc (66 mg, 0.58 mmol). The solution was stirred for 1 h and coevaporated with toluene. FC (EtOAc) gave **6b** (94 mg, 0.25 mmol, 85%) as a colorless oil. R_f = 0.32 (EtOAc/MeOH 10:1). NMR: ^{1}H (300 MHz, $CDCl_3$), δ 2.33 (s, 3 H, C$\underline{H}_3$), 3.09 (t, 2 H, J = 6.5 Hz, C$\underline{H}_2$SAc), 3.58−3.74 (m, 26 H); ^{13}C (75.4 MHz, $CDCl_3$), δ 28.8, 30.6, 61.4, 69.8, 70.1, 70.3−70.5 (several peaks), 72.5, 195.5. MALDI-TOF calcd for $C_{16}H_{32}NaO_8S$, [M + Na]$^+$ 407.2; found, [M + Na]$^+$ 407.1.

20-Thio-3,6,9,12,15,18-hexaoxaeicosan-1-ol [H-(OCH$_2$CH$_2$)$_7$SH] ***6c***. Compound **6b** was deprotected according to general procedure (II). FC (EtOAc) gave **6c** (69 mg, 0.20 mmol, 82%) as a colorless oil. R_f = 0.25 (EtOAc/MeOH 10:1). NMR: ^{1}H (300 MHz, $CDCl_3$), δ 2.68 (dt, 2 H, J = 6.5, 8.2 Hz, C$\underline{H}_2$SH), 3.53−3.76 (m, 26 H); ^{13}C (75.4 MHz, $CDCl_3$), δ 24.4, 61.8, 70.4, 70.4, 70.6−70.7 (several peaks), 72.6, 73.0. MALDI-TOF calcd for $C_{14}H_{30}NaO_7S$, [M + Na]$^+$ 365.2; found, [M + Na]$^+$ 365.1.

Self-Assembled Monolayer Preparation. Substrates used for the SAMs were prepared by evaporating a 25 Å titanium adhesion layer followed by a 2000 Å thick gold film deposition on standard silicon (100) wafers using an electron beam deposition system, Balzers UMS 500 P. The base pressure was 10^{-9} mbar and the evaporation pressure about 10^{-7} mbar. Evaporation of gold at a rate of 10 Å/s yielded a polycrystalline gold film that was heavily dominated by (111) texture.[32] The gold surfaces were, prior to SAM formation, cleaned in a 5:1:1 mixture of deionized water (Milli-Q), 25% hydrogen peroxide, and 30% ammonia, for 5 min at 80 °C, followed by extensive rinsing in deionized water and drying in N_2 gas. The efficiency of surface cleaning was immediately examined by optical characterization of the gold surface by null ellipsometry. The clean gold surfaces were then immersing to the chosen thiol solution (20 μM in ethanol) for at least 24 h for SAM formation. Upon removal, the samples were rinsed in

dx.doi.org/10.1021/jp212400z | J. Phys. Chem. C 2012, 116, 12008−12016

ethanol, ultrasonicated for 5 min, and rinsed again. Finally, they were dried in a nitrogen gas flow and immediately analyzed by ellipsometry, contact angle goniometry, and FTIR spectroscopy.

Ellipsometry. Single-wavelength null ellipsometry using a He−Ne laser light source, λ = 632.8 nm, at an angle of incidence of 70°, was used to determine thicknesses of the SAMs by means of an automatic Rudolph Research AutoEL ellipsometer software. The refractive index of a cleaned gold surface was determined and used as input values for the estimation of SAM thickness. The average value of the refractive index (3 spots on each sample) was used in a model ambient/organic film/gold, assuming an isotropic, transparent organic layer with the refractive index of n = 1.5. The film thickness was calculated as an average of measurements at three different spots at least three samples for each compound.

Contact Angle Goniometry. A semiautomatic contact angle goniometer (KSV CAM 200) was used to determine advancing and receding contact angles of water on the SAMs. As the water drop was dispensed onto the surface and expanded, the advancing contact angle was measured quasi-statically. Similarly, the receding contact angle was measured by partially withdrawing the drop back into the syringe. The data reported herein are average values of four samples. Two to three measurements were made on each sample, and each measurement consisted of three to five images for the advancing and receding angles, respectively.

Infrared Reflection Absorption Spectroscopy. The infrared reflection−absorption spectra were recorded using a Bruker IFS 66 system equipped with a reflection accessory aligned at 85° and a MCT detector. The sample chamber was continuously purged with dry N_2 to remove water vapor and carbon dioxide. All spectra were acquired at 2 cm^{-1} resolution by averaging 3000 consecutive scans. A three-term Blackmann−Harris apodization function was applied to the interferograms before Fourier transformation. A background spectrum R_0 was recorded using the self-assembly of deuterated hexadecanethiolate, $HS(CD_2)_{15}CD_3$, on gold. The sample spectra R were recorded under identical equipment conditions to yield the $-\log(R/R_0)$ spectra.

RESULTS AND DISCUSSION

Optimized geometries of SAM constituents HS-EG_nR, their vibrational frequencies, and transition dipole moments were obtained by the BP86 DFT method using the 6-31G* basis set. The extended basis set 6-311++** as well as the use of PBEPBE and Hartree−Fock with MP2 corrections were also tested for HS-$EG_{n=5,6}CH_3$ and HS-$EG_{n=5,6,7}H$, but they gave only marginal corrections to the results presented herein.

SAM Thicknesses and Contact Angles. Null ellipsometry was used to determine the thicknesses of the HS-$(CH_2CH_2O)_nR$ self-assemblies (abbreviated bellow as EG_nR), with R = CH_3, H and n = 5, 6, 7. The experimental data was compared with estimates of the SAM thicknesses based on theoretical modeling of in-SAM molecular geometry and orientation. The thicknesses of the EG_nR SAMs were calculated for the optimized geometries (with S−H bond replaced by an S−Au bond) and for the two molecular orientations shown in Figure 1. Table 1 summarizes measured and calculated SAM thicknesses. In the third column of the table, rotation angle ψ = 150° (n = 5), 50° (n = 6), and 310° (n = 7) for EG_n-CH_3 SAMs, and ψ = 140° (n = 5), 50° (n = 6), and 310° (n = 7) for EG_n-H SAMs. Smaller (larger) number in each row indicates the minimum (maximum) thickness that can be obtained by changing the rotation angle. Molecular length is defined as the distance between sulfur and H end atom; Au−S = 2.5 Å. The line connecting S and H end atoms is close to, but not exactly parallel to, the helix axis. This axis is parallel to the substrate normal at θ = 0. The choice of molecular axes and definition of Euler angles is the same as in refs 13 and 14. It is evident that the experimentally observed thicknesses agree with the theoretical estimates. The advancing and receding contact angles are also shown in Table 1. The contact angles are in line with those obtained for analogous compounds.[8,11] It is also noted that the contact angles vary marginally between the three CH_3-terminated SAMs, and the same applies for the three OH-terminated SAMs.

Table 1. Measured and Calculated SAM Thicknesses in Å

SAM	measured thickness ± SD	thickness for θ = 20° and different ψ	thickness for θ = 0	molecular length +2.5 Å	contact angles θ_a/θ_r (±1) [deg]
EG_5CH_3 (**1c**)[a]	17.3 ± 0.6	15.7 < 17.9 < 18.8	18.2	18.8	71/67
EG_6CH_3 (**2c**)	19.8 ± 0.5	18.7 < 21.5 = 21.5	21.0	21.5	72/67
EG_7CH_3 (**3c**)	24.1 ± 0.5	22.0 < 22.8 < 23.0	23.8	23.8	68/63
EG_5H (**4c**)	17.9 ± 0.6	14.9 < 16.9 < 17.7	17.2	17.8	28/20
EG_6H (**5c**)	19.5 ± 0.1	17.5 < 20.3 = 20.3	20.0	20.4	31/23
EG_7H (**6c**)	22.6 ± 0.2	20.8 < 21.3 < 22.2	22.8	22.9	31/21

[a]Labels *nc*, n = 1−6, refer to products in the experimental section (Scheme 1).

Molecular Orientation. The molecular orientation shown with zero tilt, θ = 0, is most often taken for granted in discussions concerning surface and spectral properties of OEG-terminated SAMs.[8−12,18,33] By comparing thicknesses estimated for CH_3- and H-terminated molecules with upright and tilted EG_n helix axes with the corresponding experimental values, one immediately comes to the conclusion that both orientations of SAM constituents agree equally well within experimental accuracy. Thus, ellipsometry alone cannot be used to distinguish between an upright or tilted orientation.

A perpendicular position of OEG axis with respect to the SAM supporting surface implies that symmetric CH_2-stretching vibrations, which are known to have practically zero z-component of their transition dipole moments (TDMs) (confirmed in our BP86 and HF-MP2 calculations[13]), should cancel in the IR-RA spectra due to the metal surface selection rule. This is definitely not the case as can be seen in the right panels of Figure 2, where the symmetric stretching (ν^s) vibrations contribute to a distinct shoulder at about 2865 cm^{-1} regardless of chain length. The admittance of tilted molecular orientation within the OEG SAMs considerably improves the agreement between the experimental (upper panels) and calculated (lower panels) IR-RA spectra, Figure 2. It is also worth mentioning that the assumption of zero tilt and zero rotation implies a substantial reorientation of terminal groups upon changing the chain length n by one EG unit. This seems unlikely since the surface characteristics (e.g., the wetting properties) and the relative intensity distribution of the in-chain CH_2- and terminal CH_3-stretching vibrations (and the projection of their TDMs on the surface normal) in the IR-

dx.doi.org/10.1021/jp212400z | J. Phys. Chem. C 2012, 116, 12008−12016

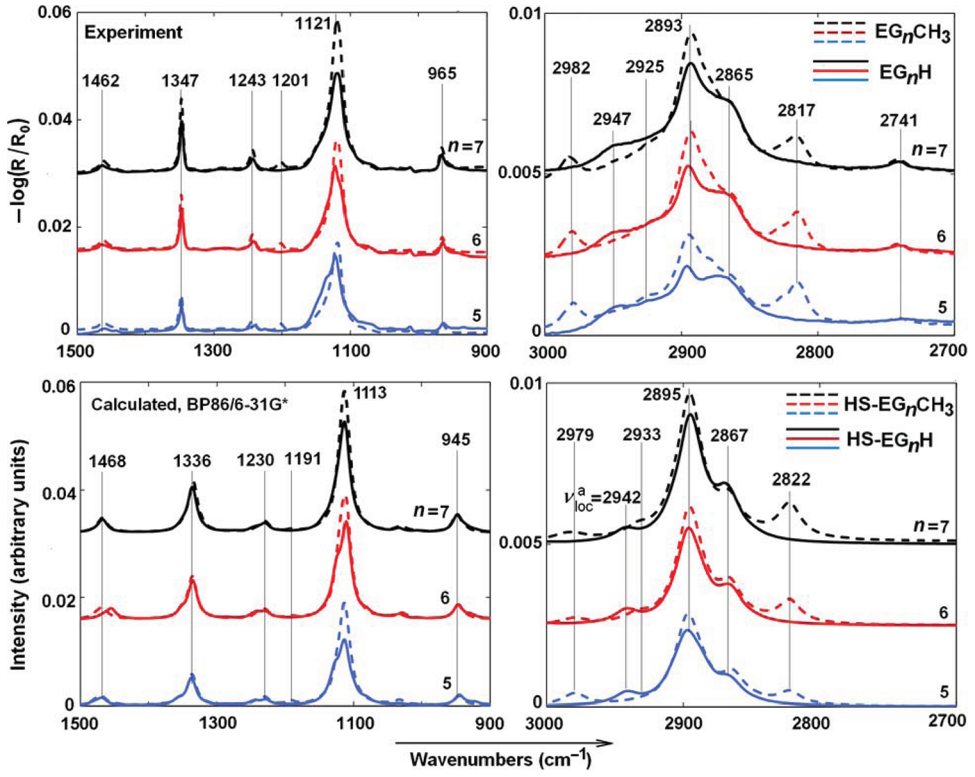

Figure 2. Measured (upper row) and model (lower row) IR-RA spectra of OEG SAMs in the fingerprint (on the left) and CH-stretching (on the right) frequency regions. The correspondence of line styles and colors is as follows: solid, H-terminus; dashed, CH_3-terminus, blue, n = 5; red, n = 6, black, n = 7. In the model spectra, the molecule tilt angle θ = 20° for all molecules; rotation angle ψ = 140° (H terminus) and 150° (CH_3 terminus) for n = 5, ψ = 50° for n = 6, and ψ = 310° for n = 7; HWHM = 8 cm^{-1} (10 cm^{-1}) for the fingerprint (CH-stretching) region. Frequency scaling factors are $\nu = 0.9747\nu_{calc}$ for CH_3 symmetric (r^+) and in-plane asymmetric stretching (r_{ip}^-) and $\nu = 0.9911\nu_{calc}$ for CH_2 symmetric (ν^s) and asymmetric (ν^a) stretching. All other characteristic frequencies (including $\nu_{loc}{}^a$ = 2942 cm^{-1}, local CH_2 asymmetric vibration) are not scaled.

RA spectra are practically the same for the SAMs with different numbers of EG units, Table 1 and Figure 2.

An alternative molecular orientation that keeps the terminal groups for the two sets of SAMs in the same orientation is shown on the right in Figure 1. The indicated constant tilt angle ~20° and rotation angles ψ for each n within the series HS-EG_nCH_3 and HS-EG_nH were obtained from the requirement of the best fit of model IR-RA spectra to experimental observations. As can be seen by adding one EG unit and simultaneously changing ψ by about −100° preserves the headgroup orientation. This is consistent with seven consecutive ($4\pi/7$) turns per period in the infinite ethylene-glycol chain.

In summary, although the thicknesses calculated for all tested in-SAM molecular orientations agree with measurements equally well, we give the preference to the tilted one, where the headgroup orientation is preserved. Otherwise, it would be very difficult to explain the nearly identical surface properties of OEG SAMs with different thicknesses, and the observed similarity of the CH_2 and CH_3 signatures in IR-RA spectra of these SAMs. Thus, the model and experimental IR-RA spectra can be agreed if, and only if, a tilted orientation of HS-EG_nR molecules is admitted. The results of modeling under the assumptions outlined above are discussed in the following section.

Measured and Model Spectra. Experimental and model IR-RA spectra of SAM series EG_nCH_3 and EG_nH are represented in Figure 2. The measured spectra are shown in the upper panels, for the fingerprint frequency region on the left and the CH-stretching on the right. The spectra for hydrogen-terminated SAMs (solid lines) are compared with the spectra measured for methyl-terminated SAMs shown by dashed lines. Different colors identify SAMs with n = 5, 6, 7. The same correspondence of colors and line styles is used in the presentation of model spectra calculated for the respective SAM constituents HS-EG_nH and HS-EG_nCH_3. These are shown in the lower panels of the figure. HS in Figure 2 is added to distinguish the calculated, single molecule spectra from the measured SAM spectra. The convention EG_nR = SAM and HS-EG_nR = molecule is also used throughout the discussion.

The presented data highlights the dependence of the number and shape of the characteristic bands on the OEG length and terminus. The information extracted from Figure 2 provides important references for the interpretation of infrared response of more complex OEG-containing SAMs such as self-assemblies of bridged oligo(ethylene glycol) and alkanethiol compounds[10−12,17,18] and modular SAMs composed of alkyl, amide, and OEG units.[16]

Earlier assignments of OEG contributions to the SAM spectra[9−12,18,33] were based on references to the parallel bands in the polarized infrared spectrum of crystalline polyethylene glycol (PEG) obtained for the electric vector parallel to the helix axis.[34,35] Here, we take advantage of ab initio modeling that allows us to distinguish the collective vibrations of the EG_n oligomers (similar to PEG polymer fundamental modes) from local vibration modes associated with the terminus groups. Also, our calculations predict relative intensities of all

dx.doi.org/10.1021/jp212400z | J. Phys. Chem. C 2012, 116, 12008−12016

Table 2. Observed/Calculated Vibration Frequencies (in cm^{-1}), Absolute Values of TDM Components (Arbitrary Units), and Assignment for EG_nH SAMs

EG_nH	$\|\mu_x\|$	$\|\mu_y\|$	$\|\mu_z\|$	assign	PEG[a], ref 34	PEG, ref 35
965/948	0.2	0.6	10.0	rock	963(s)/900	958(s)/884
1119/1112,1114	2.1,0.7	2.0,0.1	17.6,15.6	COC + rock	1102(vs)/1039	1103(vs)/1061
1243/1230	0.6	0.1	6.7	twist	1244(m)/1299	1240(m)/1280
1347/1336	0.9	0.3	15.8	wagg	1345(s)/1347	1342(s)/1386
1462/1467	0.4	0.3	7.6	bend	1457,1463(m)/1466	1454,1461(m)/1470

[a]Frequencies of parallel bands in polyethylene glycol; (vs), (s), and (m) = very strong, strong, and medium.

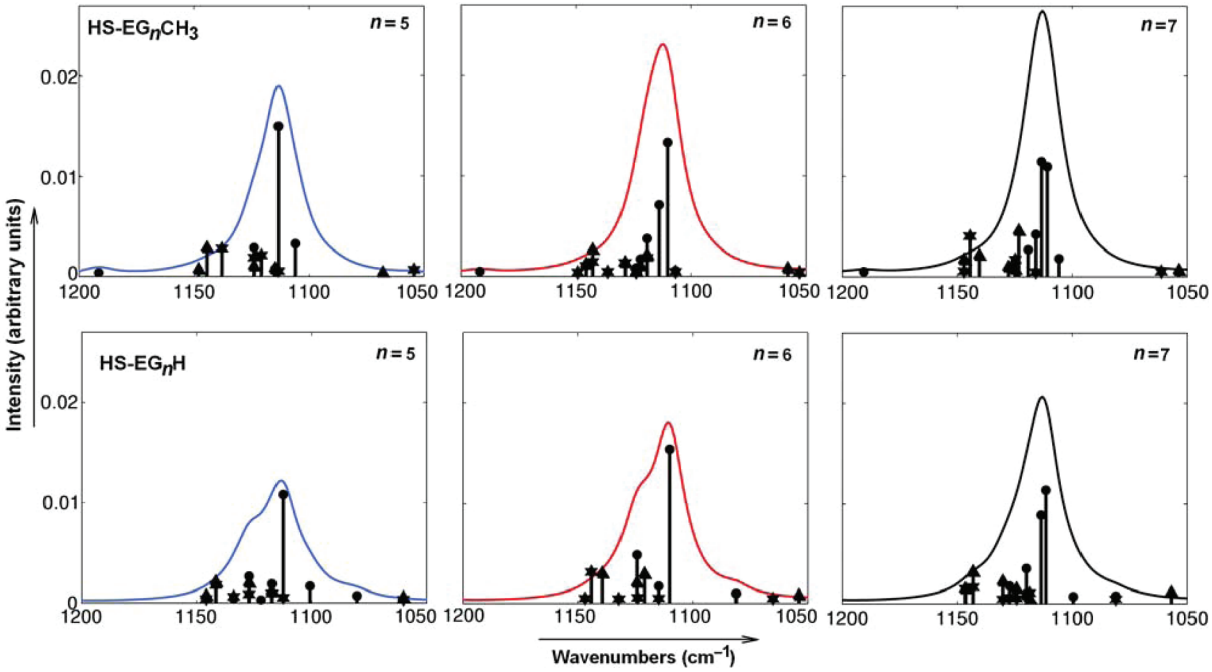

Figure 3. Mode structure of COC band as it appears in molecules $HS\text{-}EG_nCH_3$ (upper panels) and $HS\text{-}EG_nH$ (lower panels). Solid curves repeat the shape of this band in model spectra shown in Figure 2. Vertical bars headed by stars, triangles, and filled circles indicate the relative magnitude of *x*-, *y*-, and *z*-components of the largest TDMs (in molecular coordinates), respectively. The band shape is calculated by summation of Lorentzian curves centered at mode frequencies ν_i and weighted in proportion to the squared TDM projection $\mu_\perp^{(i)} = -\mu_x^{(i)} \sin\theta \cos\psi + \mu_y^{(i)} \sin\theta \sin\psi + \mu_z^{(i)} \cos\theta$ onto the SAM surface normal. Modeling details are described in refs 13 and 14.

characteristic bands and their variation with the number of EG repeating units.

With the use of calculated TDMs and their orientations in the laboratory frame of reference,[14] we have identified the infrared active vibrations contributing only to parallel bands (observed in OEG-SAM spectra), only to perpendicular bands (not observed in the SAM spectra but seen in the PEG spectrum for perpendicularly polarized light), and to the bands of both types. The model IR-RA spectra are obtained from these data assuming that, for the given *n*, the tilt and rotation of EG_n chains is practically the same for both terminal groups. Furthermore, the chain rotational angle is supposed to depend on the number of EG units as it is shown in Figure 1. The agreement between the experimental and calculated spectra is very good that provides a strong support for the proposed in-SAM molecular orientation.

Before addressing characteristic bands in the fingerprint and CH-stretching regions, we draw attention to the overall change of intensity of all bands in both frequency regions under the substitution of one terminal group by another. The intensities are noticeably lower in the spectra of H-terminated SAMs. This could be caused by experimental conditions, but the model calculations confirm that, for the given length of EG_n oligomers, the intensities of vibration modes are substantially dependent on the type of molecule terminus. Most surprisingly, this effect seems to be practically independent of the oligomer length up to $n = 7$.

Fingerprint Spectra. The interrelation between OEG SAM and PEG spectra is summarized in Table 2. The DFT calculated vibration frequencies and TDMs ascribe five common bands observed in the spectra of H- and CH_3-terminated OEG-SAMs to asymmetric COC-stretching + CH_2-rocking vibrations (965 cm^{-1}), asymmetric COC-stretching vibrations (1119 cm^{-1}), CH_2-twisting vibrations (1243 cm^{-1}), CH_2-wagging vibrations (1347 cm^{-1}), and CH_2-bending vibrations (1462 cm^{-1}). This coincides exactly with the number of parallel bands and their assignment in the PEG spectrum.[34,35] The spectral positions and relative intensities of characteristic bands in the observed and calculated IR-RA spectra are in a remarkably good agreement taking into account nonscaled frequencies and only one model parameter, the HWHM = 8 cm^{-1} for all bands in this frequency region.

The weak band at 1201 cm^{-1} appears only in the spectra of CH_3-terminated OEG-SAMs. It has been assigned to CH_3 wagging−rocking local vibrations with a wagging component involving out-of-plane hydrogen atoms.[13] The absence of this

dx.doi.org/10.1021/jp212400z | J. Phys. Chem. C 2012, 116, 12008−12016

band in the IR-RA spectra of the SAMs with hydrogen terminus confirms its CH_3 origin. Except for the CH_3 end-localized vibrations, all other bands correspond to collective modes of either methylene or skeletal vibrations. Therefore, the intensity of five major bands in this region is gradually increasing with the number of EG units. In contrast, the band of local vibrations does not show any dependence on n because these vibrations are weakly coupled to the molecular chain. In the model spectra, the corresponding band appears at 1191 cm^{-1}. Its intensity is weaker than observed experimentally, and it practically disappears in the spectrum of HS-EG_7CH_3 implicitly pointing out on the surface-state dependence of these particular vibrations.

The main difference between the spectra of CH_3- and H-terminated SAMs, which is observed in the fingerprint region, concerns the shape of the dominating COC band. Distinct from a symmetric form of this band in the EG_nCH_3 spectra for all given values of n, a kind of unresolved shoulder appears at the *high-frequency* side of the main COC band in the EG_5H spectrum. This feature migrates to the *low-frequency* side in EG_6H, and it disappears in the EG_7H spectrum, where the shape of COC band is similar to that is observed in the spectrum of EG_7CH_3 SAM. The disappearance of the shoulder is in agreement with our modeling. However, the modeling predicts the shoulder on the high frequency side of the main COC band for both EG_5H and EG_6H SAMs. It is interesting to note that, in the spectra recorded earlier for OEG-containing self-assemblies of HS-$(CH_2)_3EG_{n=6,8}H$[36] and $A_{15}EG_nH$ (A_{15} = HS-$(CH_2)_{15}CONH$, n = 6, 8, 10, 12),[11,12,17] the COC band in the IR-RA spectra of SAMs with shorter OEG ($n \leq 6$) display a shoulder on the *high-frequency* side, i.e., it is observed on the same side of main band as in the spectrum of SAM EG_5H. The reason why this shoulder occurs on the other side of the COC band in the EG_6H spectrum remains unclear.

As shown in our previous report,[15] the shape of the COC band relies on contributions from several skeletal vibration modes. The mode number, frequency, and intensity depend on the number of EG units and the type of terminal group. The multimode structure of the COC band calculated for HS-EG_nCH_3 and HS-EG_nH, n = 5, 6, 7, and the contributions of different modes into the apparent band shape is illustrated in Figure 3. It is noteworthy that the largest TDMs of COC vibration modes display the largest z-component, whereas x- and y-components are much smaller. The number of main contributing modes and their average intensity increases with the number of EG units. Thereby, the integral intensity of the COC band remains appreciably smaller for HS-EG_nH but with a clear trend toward equalizing at large n. Since the spacing between most intense modes diminishes with n, as confirmed by DFT calculations up to n = 12,[17] it explains the practically symmetric appearance of the COC band in EG_n-containing SAMs with $n \geq 7$. As seen in Figure 3, it is just the large mode spacing and specific intensity distribution that produce the shoulder of the main COC band in SAMs $EG_{n=5,6}H$.

CH-Stretching Spectra. Four and six bands are observed in the CH-stretching region of, respectively, the H- and CH_3-terminated OEG SAMs. Three of them, at 2741, 2865, and 2893 cm^{-1}, are common for both types of SAMs (emphasized by label R in Table 3). These bands can be recognized as the counterparts of bands observed at approximately the same frequencies in the PEG spectrum.[34,35] Three additional bands in methyl-terminated SAM spectra, one low- and two high-frequency side bands, were previously observed in $EG_{n=5,6}CH_3$ spectra[9] and assigned to CH_3 symmetric vibrations (2820 cm^{-1}) and two asymmetric vibrations, out-of-plane (2925 cm^{-1}) and in-plane (2983 cm^{-1}). A new feature, which is characteristic only for EG_nH spectra, appears as a weekly resolved band at 2947 cm^{-1}.

Table 3. Observed and Calculated Frequencies (in cm^{-1}) and Assignment of Characteristic Bands in CH-Stretching Region

EG_nR	calculated (not scaled)	assignment	$\|\mu_x\|$	$\|\mu_y\|$	$\|\mu_z\|^b$
2741 (R)	2755 = 1285 + 1470	comb. twist + bend			
2817 (CH_3)	2896	r^+			
2865 (R)	2890[a]	ν^s	11.1	11.2	0.5
	2892[a]	ν^s	9.2	9.4	3.8
	2840 = 1362 + 1478	ν_{comb} − comb. wagg + bend			
2893 (R)	2910[a]	ν^a	13.0	2.9	2.1
	2922[a]	ν^a	0.8	2.1	15.7
2925 (CH_3)	2933	r_{op}^-			
2947 (H)	2942	$\nu_{loc}{}^a$			
2982 (CH_3)	3056	r_{ip}^-			

[a]Frequencies of the two most intense modes in Figure 4. [b]Absolute values of TDM components are given for molecule HS-EG_7CH_3.

Over decades, the two maxima dominating the region of CH_2 stretching vibrations were associated with *symmetric* modes (ν^s),[4,10−12,18,34] which were assumed to overlap with combination vibrations (ν_{comb}),[34] Table 3. The observed and calculated band frequencies and their assignment represented in this table give a new interpretation which is, in part, complementing, and in the other part, alternative.

A comparison of measured and calculated spectra (detailed in Figure 4 by the mode intensity distribution) identifies the main feature at 2893 cm^{-1} with *asymmetric* vibration modes (ν^a). At least one of these modes has a large absolute value of the TDM z-component. In contrast, the values of $|\mu_z^s|$ for all symmetric modes are small. The physical reason for this is that the HCH-angle bisect of all CH_2 groups has nearly perpendicular orientation with respect to the helix axis. Thus, in the range of thinkable tilts and rotations of molecular constituents in SAMs EG_nR, the dominant contribution to the band at 2893 cm^{-1} comes from CH_2 *asymmetric* stretching vibrations.

Assuming that the $D(4\pi/7)$ symmetry of PEG and corresponding selection rules for higher-order excitations[37] are applicable for EG_n oligomers, the shoulder at 2865 cm^{-1} and the weak band at 2741 cm^{-1} could be interpreted as combination bands of CH_2 wagging + bending and twisting + bending vibrations, respectively. Indeed, the calculated frequencies of combination members, 1470 and 1478 cm^{-1}, 1362 cm^{-1}, and 1285 cm^{-1} for two bending, wagging, and twisting vibrations agree very well with the perpendicular bands of the PEG spectrum at 1470, 1364, and 1283 cm^{-1}.[34] Besides, the calculated values of $|\mu_x|$ and $|\mu_y|$ for these vibrations are much larger than $|\mu_z|$. This comparison does *validate* the choice of infrared active and symmetry suitable vibrations but it does not *prove* the combination nature of the features in focus. In particular, it does not prove that the shoulder at 2865 cm^{-1} is a signature of combined CH_2 wagging and bending vibrations.

On the basis of the preceding and forthcoming argumentation, we believe that the combination band of wagging and bending vibrations might contribute to the OEG SAM spectra. However, the discussed next alternative interpretation, implying

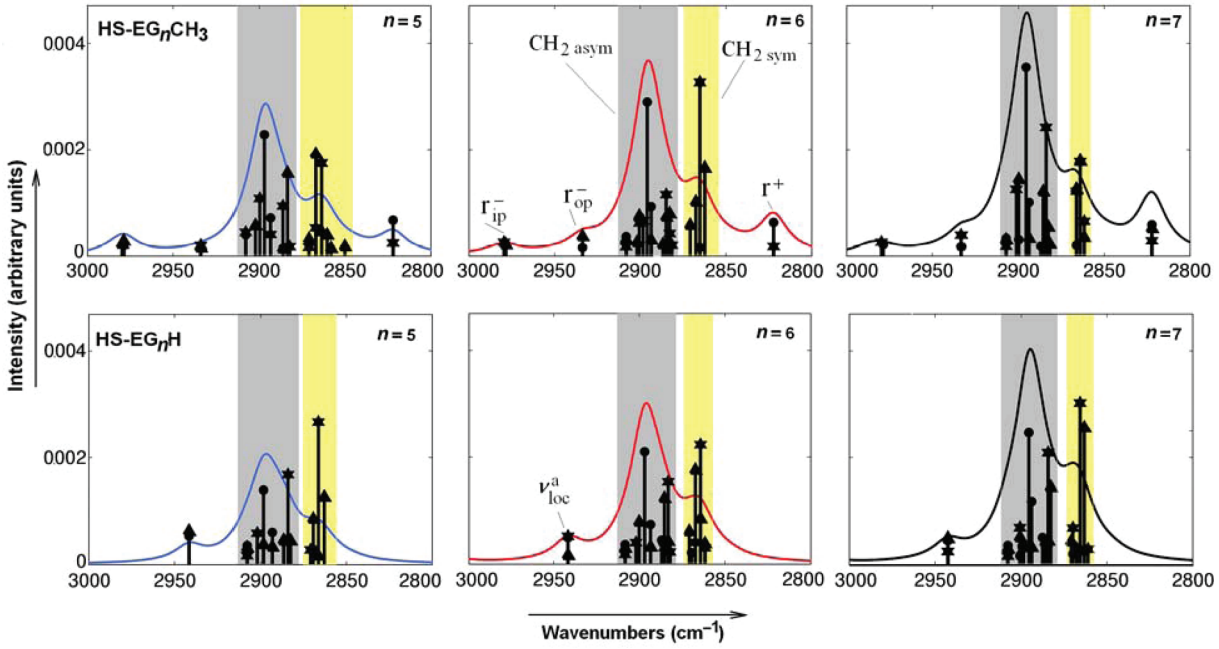

Figure 4. Mode structure of characteristic bands in the CH-stretching region. Solid curves repeat model spectra shown in Figure 2. Indication of TDM components is the same as that in Figure 3. Regions of asymmetric (ν^a) and symmetric (ν^s) collective CH_2-stretching vibrations are gray- and yellow-shaded. The meaning of other labels is as follows: symmetric (r^+), asymmetric out of plane (r_{op}^-) and in-plane (r_{ip}^-) stretching vibrations of CH_3, and ν_{loc}^a asymmetric stretching vibrations of CH_2 group adjacent to O−H.

the dominant role of collective methylene symmetric vibrations in the formation of shoulder at 2865 cm^{-1}, seems more plausible.

A conceivable tilt of OEG axis within studied SAMs by about 20° suggests an assignment documented in Table 3 and illustrated in Figure 4. It is seen that symmetric vibration modes with large *x* and *y* TDM components can reveal themselves as an unresolved ν^s band that looks as a low frequency shoulder of ν^a band. This makes the shape of HS-EG_nR spectra (calculated) very much similar to that we see in the EG_nR SAM spectral series (measured) represented in Figure 2. In particular, the calculated reduction of spectral intensity of HS-EG_nH bands in comparison with HS-EG_nCH_3 bands (apparently more strong for ν^a than for ν^s band) agrees well with experimental observations. Thus, the broad band with shoulder dominating the region of methylene stretching vibrations can be thought resulting from an overlap of bands ν^a and ν^s (observed as the main peak and shoulder, respectively) with some admixture of wagging + bending combination band.

The CH_3 infrared activity is well-known,[8−10,18,36,38−40] and the spectral signatures of CH_3 stretching vibrations in OEG SAM spectra have been previously discussed by us in great detail.[13] The vibration frequency of O−H terminus is far away from the region in focus. Therefore, the weakly resolved band at 2947 cm^{-1} in EG_nH spectra may seem puzzling. Our calculations show, however, that such a satellite band has to be present at frequency ν_{loc}^a = 2942 cm^{-1}.

As we noticed previously,[16] the vibrational spectrum of SAMs terminated by an extended alkyl chain $(CH_2)_nH$ contains a specific mode of CH_2 symmetric stretching vibrations (d_{loc}^+ = 2938 cm^{-1}), almost completely localized at the first methylene group. The mode ν_{loc}^a, which was observed in this work for the first time, corresponds to intense asymmetric stretching vibrations of the next to end-oxygen methylene group, while other molecular atoms remain essentially immovable. The nature of local excitations d_{loc}^+ and ν_{loc}^a is common. Both are caused by an end defect. In the alkane chain, it is CH_3 end group; in OEG chain, it is end hydrogen atom. The observed constancy of the ν_{loc}^a band intensity for *n* = 5, 6, 7 and the absence of a similar band in EG_nCH_3 spectra strongly favor the assignment of the band at 2947 cm^{-1} to *local asymmetric stretching vibrations* of methylene closest to the SAM surface.

It is worth noting that, in ref 39, a specific CH_2 stretching frequency was ascribed to methylene adjacent to the methyl end group on phenomenological grounds. In that case, the authors of quoted work were interpreting the sum frequency spectra of *n*-alkanethiol monolayers. This indicates that the presence of localized vibrations in SAM IR spectra is a common phenomenon deserving particular attention.

■ CONCLUSIONS

We have undertaken a systematic study of two series of self-assembled monolayers on gold and methyl- and hydrogen-terminated OEG thiols HS-$(CH_2CH_2O)_nCH_3$ and HS-$(CH_2CH_2O)_nH$, with *n* = 5, 6, and 7. Among others, we have addressed the following questions: (i) is the OEG chain tilted, and if that is the case, how large is the tilt? (ii) Is the headgroup orientation dependent on the OEG length? Our answers to these questions are (i) the tilt is substantial, about 20°, and (ii) the orientation of the terminal groups does not change with OEG length.

Several pro-arguments are presented in the above discussion for a tilted orientation. The most convincing argument in favor of substantial OEG axis tilt is that it establishes quantitative correspondence between the shape and intensity of all observed bands in the IR-RA spectra and the ab initio calculated spectra of SAM molecular constituents. The previous interpretation of IR response in the high frequency region goes back to Miyazawa et al.'s work.[34] It is based on speculative assumptions regarding the contribution of higher order excitations.

dx.doi.org/10.1021/jp212400z | J. Phys. Chem. C 2012, 116, 12008−12016

Unfortunately, these have never been evaluated quantitatively. The results of linear response modeling presented here do not deny that contribution but clearly indicate that the OEG SAMs spectral appearance in the frequency region 2850−2950 cm^{-1} can be well and exhaustively explained, except the band at 2741 cm^{-1}. Also, we draw attention to a useful byproduct of this study, a weak band at 2947 cm^{-1} (calculated at 2942 cm^{-1}) that is characteristic for H-terminated but not CH_3-terminated OEG SAMs. In the spectra of more conventional SAMs containing long alkyl chains, this feature is hidden. Taken together, the presented results provide a platform for further studies of modular and complex OEG-containing SAMs.

AUTHOR INFORMATION

Corresponding Author

*Phone: +46 (0)13 281877. Fax: +46 (0)13 281399. E-mail: bolie@ifm.liu.se.

Notes

The authors declare no competing financial interest.

ACKNOWLEDGMENTS

This work was supported by the Visby program of the Swedish Institute (to S.I.) and the Swedish Research Council (to V.R.). R.V. also acknowledges the support from the Research Council of Lithuania (MIP-098/2011).

REFERENCES

(1) Pale-Grosdemange, C.; Simon, E. S.; Prime, K. L.; Whitesides, G. M. *J. Am. Chem. Soc.* **1991**, *113*, 12−20.
(2) Prime, K. L.; Whitesides, G. M. *Science* **1991**, *252*, 1164−1167.
(3) Prime, K. L.; Whitesides, G. M. *J. Am. Chem. Soc.* **1993**, *115*, 10714−10721.
(4) Harder, P.; Grunze, M.; Dahint, R.; Whitesides, G. M.; Laibinis, P. E. *J. Phys. Chem. B* **1998**, *102*, 426−436.
(5) Lahiri, J.; Isaacs, L.; Tien, J.; Whitesides, G. M. *Anal. Chem.* **1999**, *71*, 777−790.
(6) Vanderah, D. J.; La, H. L.; Naff, J.; Silin, V.; Rubinson, K. A. *J. Am. Chem. Soc.* **2004**, *126*, 13639−13641.
(7) Skoda, M. W. A.; Jacobs, R. M. J.; Willis, J.; Schreiber, F. *Langmuir* **2006**, *23*, 970−974.
(8) Vanderah, D. J.; Valincius, G.; Meuse, C. W. *Langmuir* **2002**, *18*, 4674−4680.
(9) Vanderah, D. J.; Arsenault, J.; La, H.; Gates, R. S.; Silin, V.; Meuse, C. W.; Valincius, G. *Langmuir* **2003**, *19*, 3752−3756.
(10) Wang, R. Y.; Himmelhaus, M.; Fick, J.; Herrwerth, S.; Eck, W.; Grunze, M. *J. Chem. Phys.* **2005**, *122*, 164702−6.
(11) Valiokas, R.; Svedhem, S.; Svensson, S. C. T.; Liedberg, B. *Langmuir* **1999**, *15*, 3390−3394.
(12) Valiokas, R.; Östblom, M.; Svedhem, S.; Svensson, S. C. T.; Liedberg, B. *J. Phys. Chem. B* **2000**, *104*, 7565−7569.
(13) Malysheva, L.; Onipko, A.; Valiokas, R.; Liedberg, B. *J. Phys. Chem. B* **2005**, *109*, 13221−13227.
(14) Malysheva, L.; Onipko, A.; Valiokas, R.; Liedberg, B. *J. Phys. Chem. A* **2005**, *109*, 7788−7796.
(15) Malysheva, L.; Onipko, A.; Liedberg, B. *J. Phys. Chem. A* **2008**, *112*, 728−736.
(16) Lee, H. H.; Ruzele, Z.; Malysheva, L.; Onipko, A.; Gutes, A.; Bjorefors, F.; Valiokas, R.; Liedberg, B. *Langmuir* **2009**, *25*, 13959−13971.
(17) Valiokas, R.; Malysheva, L.; Onipko, A.; Lee, H. H.; Ruželė, Ž.; Svedhem, S.; Svensson, S. C. T.; Gelius, U.; Liedberg, B. *J. Electron Spectrosc. Relat. Phenom.* **2009**, *172*, 9−20.
(18) Valiokas, R.; Svedhem, S.; Östblom, M.; Svensson, S. C. T.; Liedberg, B. *J. Phys. Chem. B* **2001**, *105*, 5459−5469.
(19) Zorn, S.; Skoda, M. W. A.; Gerlach, A.; Jacobs, R. M. J.; Schreiber, F. *Langmuir* **2011**, *27*, 2237−2243.
(20) Schwendel, D.; Hayashi, T.; Dahint, R.; Pertsin, A.; Grunze, M.; Steitz, R.; Schreiber, F. *Langmuir* **2003**, *19*, 2284−2293.
(21) Zorn, S.; Martin, N.; Gerlach, A.; Schreiber, F. *Phys. Chem. Chem. Phys.* **2010**, *12*, 8985−8990.
(22) Kankate, L.; Werner, U.; Turchanin, A.; Gölzhäuser, A.; Großmann, H.; Tampé, R. *Biointerphases* **2010**, *5*, 30−36.
(23) Cheung, C. L.; Camarero, J. A.; Woods, B. W.; Lin, T. W.; Johnson, J. E.; De Yoreo, J. J. *J. Am. Chem. Soc.* **2003**, *125*, 6848−6849.
(24) Nilebäck, E.; Westberg, F.; Deinum, J.; Svedhem, S. *Anal. Chem.* **2010**, *82*, 8374−8376.
(25) Nilebäck, E.; Feuz, L.; Uddenberg, H.; Valiokas, R.; Svedhem, S. *Biosens. Bioelectron.* **2011**, *28*, 407−413.
(26) Benesch, J.; Svedhem, S.; Svensson, S. C. T.; Valiokas, R.; Liedberg, B.; Tengvall, P. *J. Biomater. Sci., Polym. Ed.* **2001**, *12*, 581−597.
(27) Saalmink, M.; van der Marel, C.; Stapert, H. R.; Burdinski, D. *Langmuir* **2006**, *22*, 1016−1026.
(28) Bouzide, A.; Sauvé, G. *Org. Lett.* **2002**, *4*, 2329−2332.
(29) Ghosh, S.; Ramakrishnan, S. *Macromolecules* **2005**, *38*, 676−686.
(30) Boden, N.; Bushby, R. J.; Clarkson, S.; Evans, S. D.; Knowels, P. F.; Marsh, A. *Tetrahedron* **1997**, *53*, 10939−10952.
(31) Jeong, K. S.; Cho, Y. L.; Pyun, S. Y. *Tetrahedron Lett.* **1995**, *36*, 2827−2830.
(32) Bertilsson, L.; Liedberg, B. *Langmuir* **1993**, *9*, 141−149.
(33) Pertsin, A. J.; Grunze, M.; Garbuzova, I. A. *J. Phys. Chem. B* **1997**, *102*, 4918−4926.
(34) Miyazawa, T.; Fukushima, K.; Ideguchi, Y. *J. Chem. Phys.* **1962**, *37*, 2764−2776.
(35) Yoshihara, T.; Tadokoro, H.; Murahashi, S. *J. Chem. Phys.* **1964**, *41*, 2902−2911.
(36) Vanderah, D. J. Biochemical Science Division, National Institute of Standards & Technology, Gaithersburg, MD. Private communication, 2008.
(37) Herzberg, G. *Infrared and Raman Spectra*; D. Van Nostrad Company, Inc.: New York, 1945.
(38) Ong, T. H.; Davies, P. B.; Bain, C. D. *Langmuir* **1993**, *9*, 1836−1845.
(39) Himmelhaus, M.; Eisert, F.; Buck, M.; Grunze, M. *J. Phys. Chem. B* **2000**, *104*, 576−584.
(40) Buck, M. *Phys. Chem. Chem. Phys.* **2003**, *5*, 18−25.